Q. J. R. Meteorol. Soc. (2003), **129**, pp. 1–999

Nonlinear singular spectrum analysis of the tropical stratospheric wind

By WILLIAM W. HSIEH[1]* and KEVIN HAMILTON[2]

[1] *University of British Columbia, Canada*
[2] *International Pacific Research Center, University of Hawaii at Manoa, Hawaii*

(Received 1 September, 2001; revised 10 January 2003)

Summary

The neural network-based nonlinear singular spectrum analysis (NLSSA) is applied to the zonal winds in the 70-10 hPa region (roughly 20-30 km altitude) measured at near-equatorial stations during 1956-2000. The data are pre-filtered by the linear singular spectrum analysis (SSA), with the leading 8 SSA principal components (PCs) used as inputs for the NLSSA. The NLSSA fits a curve to the data in the 8-D PC space. This NLSSA curve when projected onto the 2-D plane spanned by any two PCs shows the relation between the two SSA PCs. As different SSA modes are associated with different time scales, the relations found by the NLSSA reveal the time scales between which there are interactions—interactions between the dominant quasi-biennial oscillation (QBO) time scale of about 28 months and the first harmonic at 14 months, and between 28 months and 12 months are found. The anharmonic nature of the QBO is well represented by the NLSSA mode 1, but not by individual SSA modes. The NLSSA is also applied to the time series of the zonal wind acceleration.

Keywords: Quasi-biennial oscillation Tropical stratosphere Neural networks

1. Introduction

In the equatorial stratosphere, the variability of the prevailing wind is dominated by an oscillation between strong westerly and easterly winds, with a quasi-biennial period. Varying from cycle to cycle, the period of this quasi-biennial oscillation (QBO) has been found to range between 22 and 33 months, with a mean value of about 28 months. The QBO dwarfs the annual cycle and other types of variability in this part of the atmosphere. Recent reviews of the QBO phenomenon include Hamilton (1998) and Baldwin et al. (2001).

From routine balloon observations up to 10 hPa (∼30 km), a standard height-time record of monthly-mean zonal wind constructed at near-equatorial stations has been assembled over the years (Naujokat 1986; Marquardt and Naujokat 1997). Earlier studies have applied various linear multivariate and time series analysis techniques to these zonal wind data. Applying principal component analysis (PCA), also known as empirical orthogonal function (EOF) analysis, Wallace et al. (1993) found that the first two principal components (PCs) (i.e. time coefficients of the PCA) were quasi-cyclic and in quadrature. Using the singular spectrum analysis (SSA) (also called space-time PCA, or extended EOF) with a window of 40 months, Fraedrich et al. (1993) and Wang et al. (1995) found that the leading two PCs were in quadrature and described an oscillation with steady downward phase propagation.

Since PCA and SSA are linear techniques, nonlinear characteristics of the QBO are missed in these studies. For instance, the leading PCA or SSA modes tend to describe near-sinusoidal oscillations rather than the more square-wave behavior manifested by the QBO. Also the leading modes capture virtually none of the asymmetry between westerly and easterly shear zones, and between westerly (i.e. eastward) and easterly (i.e. westward) acceleration regimes, characteristics which are clearly displayed by the QBO.

Recent advances in neural networks modelling have led to the nonlinear generalization of many of the classical multivariate and time series techniques. The nonlinear

* Corresponding author: Department of Earth and Ocean Sciences, University of British Columbia, Vancouver, B.C. V6T 1Z4, Canada

PCA (NLPCA) method has been applied to the study of the El Niño-Southern Oscillation (ENSO) phenomenon (Monahan 2001; Hsieh 2001). The nonlinear SSA (NLSSA) has been developed and applied to examine ENSO (Hsieh and Wu 2002). Hamilton and Hsieh (2002) used a variant of the NLPCA to analyze the zonal wind in the equatorial stratosphere — the nonlinear approach was found to give a significantly more complete characterization of the QBO behavior in a single mode, than does the comparable linear analysis.

In this paper, the NLSSA is applied to the equatorial stratospheric zonal wind data. One important aspect of the application of the NLSSA to the QBO is its use as a filter. The actual time series of the wind measured at single stations is somewhat noisy and for some applications it is desirable to have a smoother representation of the QBO time series that captures the essential features at all height levels. Examples of such applications are (i) producing time series of the QBO phase that can be correlated with other aspects of the circulation, and (ii) producing smooth series that can be used to objectively characterize the time variability of QBO amplitude and period.

The very non-sinusoidal nature of the QBO means that standard linear filtering procedures (e.g. running means or Fourier band-pass) tend to smooth out essential features of the oscillation. The NLSSA approach adopted here produces an objective representation of the filtered QBO that, while smooth, is more faithful to the actual details of QBO evolution than that produced by Fourier band-pass filtered techniques, or, as shown in this paper, linear SSA.

Section 2 gives a brief description of the SSA and NLSSA techniques. The NLSSA method is applied to the zonal wind in Section 3, and to the zonal acceleration in Section 4.

2. A brief description of the SSA and the NLSSA

The classical Fourier spectral analysis involves decomposing a time series into sinusoidal waves of various frequencies (Jenkins and Watts 1968). If the periodic signal is not of sinusoidal form, then the Fourier spectral analysis will scatter the energy of the signal into numerous frequency bands or modes. In recent years, the restriction to sinusoidal wave forms has been lifted by the SSA method (Elsner and Tsonis 1996; Ghil et al. 2002). In the SSA approach, a time series is lagged by $1, \ldots, K$ time steps. The time series and its lagged versions can be regarded as a set of variables $\{y_i\}$ $(i = 1, \ldots, K + 1)$, which can be analyzed by the familiar PCA. This resulting method is the SSA with window $L\,(= K + 1)$. In the multivariate case where there is more than one time series, one can again make lagged copies of the time series, treat the lagged copies as extra variables, and apply the PCA to this augmented dataset— resulting in the multichannel SSA (MSSA) method. For brevity, we will use the term SSA to denote both the univariate and multivariate methods. Drawbacks of the SSA method include the window choice, and the assumption that the noise in the dataset is white. There has been recent generalization of the SSA method to handle red noise (Allen and Smith 1997) and non-Gaussian data (Hannachi and Allen 2001).

In PCA, a straight line approximation to the dataset is sought which accounts for the maximum amount of variance in the data. There are now several types of neural network (NN) models which will use, instead of the straight line, a continuous curve to approximate the data. The nonlinear PCA (NLPCA) method of Kramer (1991) is capable of extracting open curve solutions to approximate the data, but not closed curve solutions. Kirby and Miranda (1996) introduced an NLPCA with a circular node at the bottleneck (henceforth NLPCA.cir), capable of extracting closed curve solutions. Both

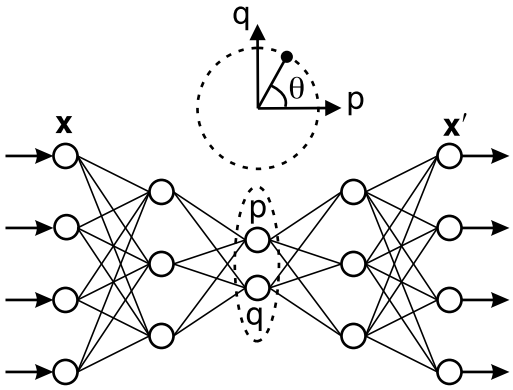

Figure 1. A schematic diagram illustrating the NN model for calculating the NLPCA with a circular node at the bottleneck (NLPCA.cir). The model is a standard feedforward NN (i.e. multi-layer perceptron), with 3 'hidden' layers of variables or 'neurons' (denoted by circles) sandwiched between the input layer $\mathbf{x}$ on the left and the output layer $\mathbf{x}'$ on the right. Next to the input layer (with l neurons) is the encoding layer (with m neurons), followed by the 'bottleneck' layer, then the decoding layer (with m neurons), and finally the output layer (with l neurons), i.e. a total of 4 layers of transfer functions are needed to map from the inputs to the outputs. In NLPCA.cir, the bottleneck contains two neurons p and q confined to lie on a unit circle, i.e. only 1 degree of freedom as represented by the angle θ. Effectively, a nonlinear function $\theta = F(\mathbf{x})$ maps from the higher dimension input space to the lower dimension bottleneck space, followed by an inverse transform $\mathbf{x}' = \mathbf{G}(\theta)$ mapping from the bottleneck space back to the original space, as represented by the outputs. Data compression is achieved by the bottleneck, yielding the nonlinear principal component (NLPC) θ. For NLSSA, the inputs to the network are simply the leading PCs from the SSA, which serves as a prefilter.

NLPCA and NLPCA.cir have been studied by Hsieh (2001), who pointed out that the general configuration of the NLPCA.cir can model not only closed curve solutions, but also open curve solutions. Hamilton and Hsieh (2002) applied the NLPCA.cir to study the QBO.

The NLPCA.cir model is described in detail in Hsieh (2001), and briefly in the Appendix here. The input data are in the form $\mathbf{x}(t) = [x_1, \ldots, x_l]$, where each variable x_i, $(i = 1, \ldots, l)$, is a time series containing n observations. The information is mapped forward through a bottleneck to the output $\mathbf{x}'$ (Fig. 1). The parameters of the network are solved by minimizing the cost function, which is basically the mean square error (MSE) of $\mathbf{x}'$ relative to $\mathbf{x}$.

Based on the NLPCA.cir, Hsieh and Wu (2002) developed the nonlinear SSA (NLSSA) method: First, SSA is used to pre-filter the data, i.e. the original data are analyzed by the SSA with window L. As in PCA, each SSA mode is a product of two components—a time coefficient, the principal component (PC), and an eigenvector of the spatial variables at various lags (also called the loading pattern). Only the first few leading SSA modes are retained, and their PCs, $x_1, \ldots, x_l$, are then served as input variables to the NLPCA.cir network (Fig. 1). The NLPCA.cir finds a continuous curve solution by nonlinearly relating the PCs, thereby giving the first NLSSA mode.

Applying the NLSSA to analyze the tropical Pacific sea surface temperature field and the sea level pressure field, Hsieh and Wu (2002) found the NLSSA to have several advantages over SSA: (a) While the PCs from different SSA modes are linearly uncorrelated, they may have nonlinear relationships that can be detected by the NLSSA. (b) Although the SSA modes are not restricted to sinusoidal oscillations in time like the Fourier spectral components, in practice they are inefficient in modelling strongly anharmonic oscillations, scattering the signal energy into many SSA modes. The NLSSA

recombines the SSA modes to extract the anharmonic signal. (c) As different SSA modes are associated with different time scales, the relations found by the NLSSA reveal the time scales between which there are interactions.

3. NLSSA of the zonal wind

The data are the monthly means of the zonal wind component measured by twice-per-day balloon ascents at: Canton Is. (2.8°S, 171.8°W, January 1956–August 1967), Gan (0.7°S, 73.2°E, September 1967–December 1975), and Singapore (1.4°N, 103.9°E, January 1976–December 2000). Belmont and Dartt (1968) found very little longitudinal variation of the QBO in the data, and examining data including the overlapped period of January 1974–December 1975 at Singapore and Gan, Naujokat (1986) found no sytematic differences that would indicate problems in concatenating the time series. Values at 70, 50, 40, 30, 20, 15 and 10 hPa (i.e. from about 20 km to 30 km altitude) are used, with the mean at each level removed (but the seasonal cycle retained).

SSA was applied to the data, with window $L = 40$ months, the same value of L chosen by Wang et al. (1995). The leading 8 modes accounted for 37.8, 36.7, 4.1, 3.8, 2.3, 1.9, 1.5 and 1.0 %, respectively, of the variance— cumulatively 89.1% of the variance. The eigenvectors of these leading 8 modes are shown in Fig. 2, and the corresponding PCs in Fig. 3. As commonly found for SSA, the modes tend to occur in pairs with similar characteristics. For instance, the first pair of modes have a time scale of about 28 months, that of the QBO. This time scale can be observed in both the first two eigenvectors (Fig. 2a and b) and the first two PCs (Fig. 3a). Modes 3 and 4 display more irregular oscillations than modes 1 and 2. Mode 5 also displays relatively irregular oscillations, while mode 6 displays oscillations at around the 15-month period. Oscillations with a period of about 14 months (the first harmonic of the 28-month period) are found in mode 7, and a period of about 12 months in mode 8.

With these 8 leading PCs serving as inputs to the NLPCA.cir network (Fig. 1), the resulting NLSSA mode 1 solution (Fig. 4) shows the dominant relation in the PC-space to be the cyclic relation between PC1 and PC2. PC3 and PC4 have essentially no relation with PC1. Increasingly strong relation with PC1 can be found as we proceed from PC5, PC6 and finally PC7. Since PC7 oscillates at the first harmonic of the QBO, it is not surprising it relates strongly to the fundamental period as represented by PC1 (and PC2). Though the curve relating PC1 and PC7 is very nonlinear, it can arise in a linear oscillatory system. Consider two harmonic time series oscillating at frequencies ω_1 and ω_2,

$$z_1(t) = A_1 \cos(\omega_1 t - \delta_1) \,, \quad z_2(t) = A_2 \cos(\omega_2 t - \delta_2) \,. \tag{1}$$

A plot of z_1 versus z_2 displays the trajectory, which forms a closed Lissajous curve if and only if ω_2/ω_1 is a rational number. The curve linking PC1 and PC7 in Fig. 4f resembles the expected Lissajous ∞-shaped curve between the fundamental frequency and the first harmonic. The plot for PC1 versus PC8 (containing annual oscillations) suggests a moderate relation between the basic QBO cycle and the annual cycle. Relations between the higher mode PCs can also be found, e.g. Fig. 4h reveals a weak cyclic relation between PC7 and PC8 .

Without running NLSSA, one could not tell simply from the scatter plots of the PCs in Fig. 4 which ones have or not have relations linked by a curve. For instance, while the NLSSA found interesting curves in Figs. 4e and f, it did not find one in Fig. 4c. What it means is that when PC1 approaches maximum or minimum values, PC4 also approaches maximum or minimum values (Fig. 4c), but in a random order, so NLSSA

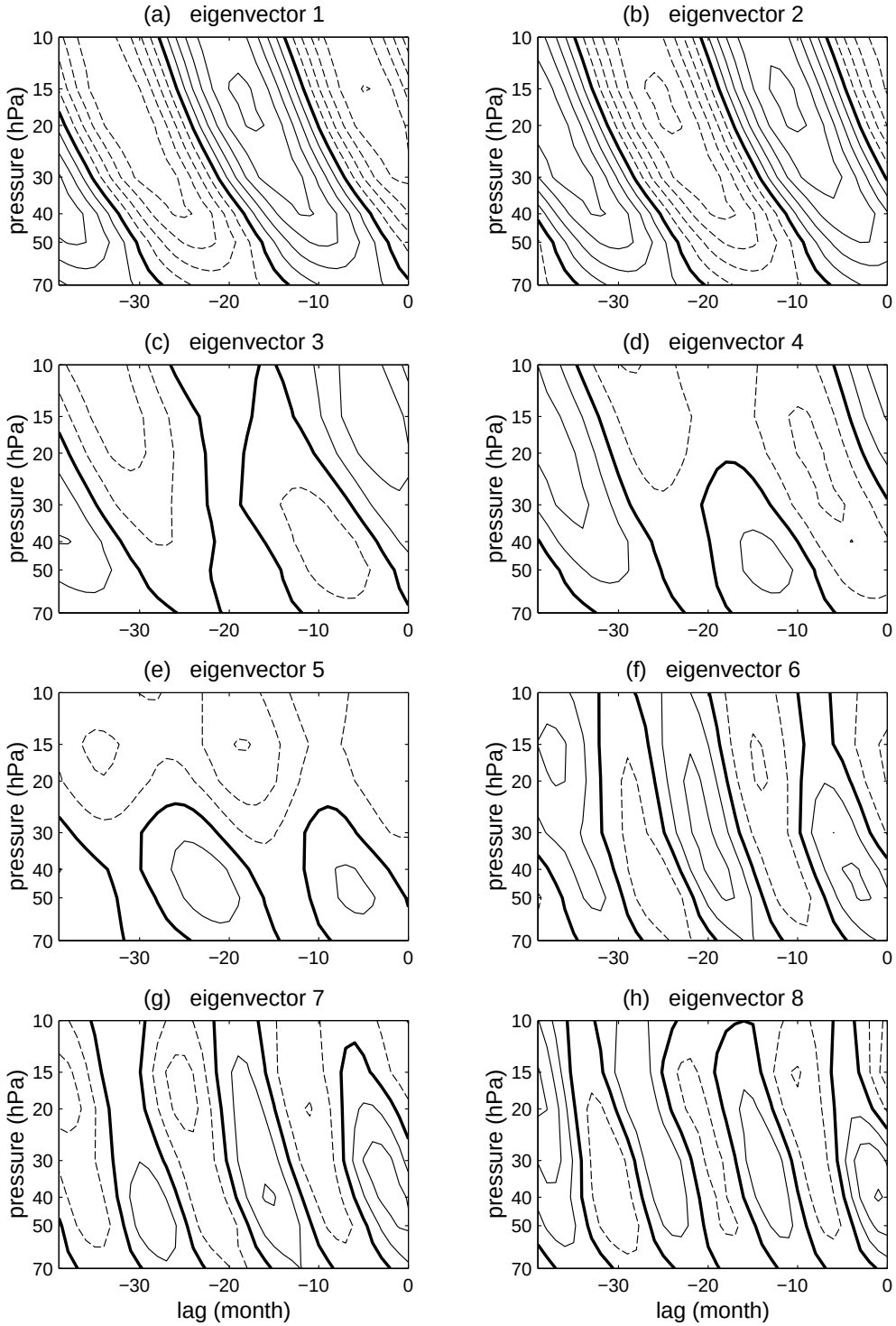

Figure 2. Contour plots of the leading eight SSA eigenvectors for the zonal wind. The horizontal axis is the lag in months. Negative contours (i.e. easterly winds) are dashed, while the zero contour is thickened. The eigenvectors are normalized to unit norm. Contour intervals are 0.02 in (a) and (b), and 0.05 in panels (c)-(h).

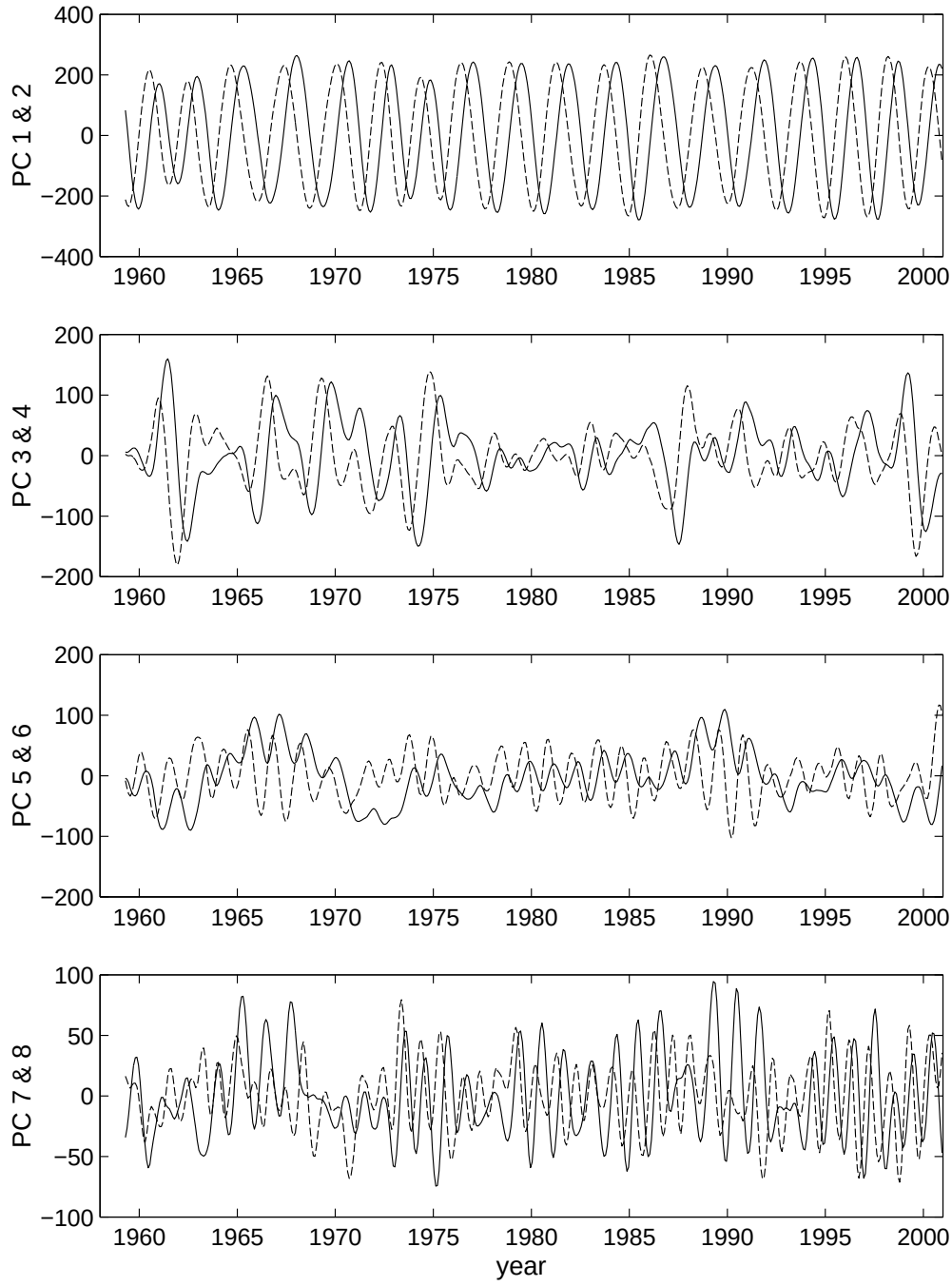

Figure 3. The leading eight SSA principal component (PC) time series (in ms^{-1}) for the zonal wind. The PCs are plotted in pairs, with those for modes 1, 3, 5 and 7 shown by solid curves, and those for modes 2, 4, 6 and 8 by dashed curves. The tick mark along the abscissa indicates the beginning of the given year.

TABLE 1. The correlation and root mean square error (RMSE) between observations and the reconstructed component (RC) from NLSSA mode 1 (NLRC1), from SSA mode 1 (RC1), and from SSA modes 1 and 2 (RC1+2).

pressure	correlation			RMSE		
(hPa)	NLRC1	RC1	RC1+2	NLRC1	RC1	RC1+2
10	0.880	0.875	0.881	9.03	12.38	9.00
15	0.900	0.895	0.897	8.75	12.50	8.83
20	0.903	0.892	0.897	8.43	12.37	8.66
30	0.918	0.893	0.905	7.13	11.60	7.62
40	0.916	0.882	0.890	6.43	10.61	7.28
50	0.896	0.855	0.856	5.91	9.05	6.83
70	0.841	0.783	0.793	3.58	4.80	4.00
average	0.894	0.868	0.874	7.04	10.47	7.46

The last row gives the average over the 7 vertical levels. The RMSE is in ms^{-1}.

could not find a deterministic relation. Similarly, Fig. 4b, which says PC3 tends to have greater variability when PC1 is near 0 is also intriguing, as no deterministic relation was detected by the NLSSA.

The time series for the nonlinear principal component θ is shown in Fig. 5a. The departure from a steady increase in θ with time, i.e. the θ anomaly, is also shown as a dashed curve. When the θ anomaly increases (decreases) with time the QBO period is anomalously short (long).

The NLSSA mode 1 space-time loading pattern for a given value of θ can be obtained by mapping from θ to the outputs $\mathbf{x}'$, which are the 8 PC values corresponding to the given θ. Multiplying each PC value by its corresponding SSA eigenvector and summing over the 8 modes, we obtain the NLSSA mode 1 loading pattern corresponding to the given θ.

Comparing the NLSSA mode 1 loading patterns for various θ values (Fig. 6) with eigenvectors 1 and 2 (Fig. 2), we note that the nonlinear mode has more asymmetry between the westerly and easterly anomalies, with the easterly anomalies penetrating further down in the atmosphere, as observed. Also in the NLSSA loading patterns, the easterly to westerly transitions are more rapid than the westerly to easterly transitions, a feature very characteristic of the raw observations in each cycle of the QBO (e.g. Naujokat, 1986).

The NLSSA reconstructed component 1 (NLRC1) is the approximation of the original 7 time series (at the 7 vertical levels) by the NLSSA mode 1. The neural network outputs $\mathbf{x}'$ are the NLSSA mode 1 approximation for the 8 leading PCs. Multiplying these approximated PCs by their corresponding SSA eigenvectors, and summing over the 8 modes allows the reconstruction of the 7 time series from the NLSSA mode 1. As each eigenvector contains the loading over a range of lags, each value in each reconstructed time series at time t_j also involves averaging over the contributions at t_j from various lags. The RC from SSA mode 1 (RC1) and SSA modes 1 and 2 (RC1+2) are also calculated. The correlation and root mean square error (RMSE) between the RCs and the observations are given in Table 1, and the RCs are plotted for the period 1981-2000 in Fig. 7. Constructing the RC by using more SSA modes will of course fit the observations better, but will be fitting to the noise in the data as well.

After the NLSSA mode 1 solution had been removed from the data (i.e. the eight PCs), the residual was input into the same NLPCA.cir network to yield NLSSA mode 2. This mode 2 solution mainly cyclically links PC3 with PC4, without much interaction with the other PCs. Thus NLSSA mode 2 was not very different from the SSA modes 3 and 4, and will not be discussed further.

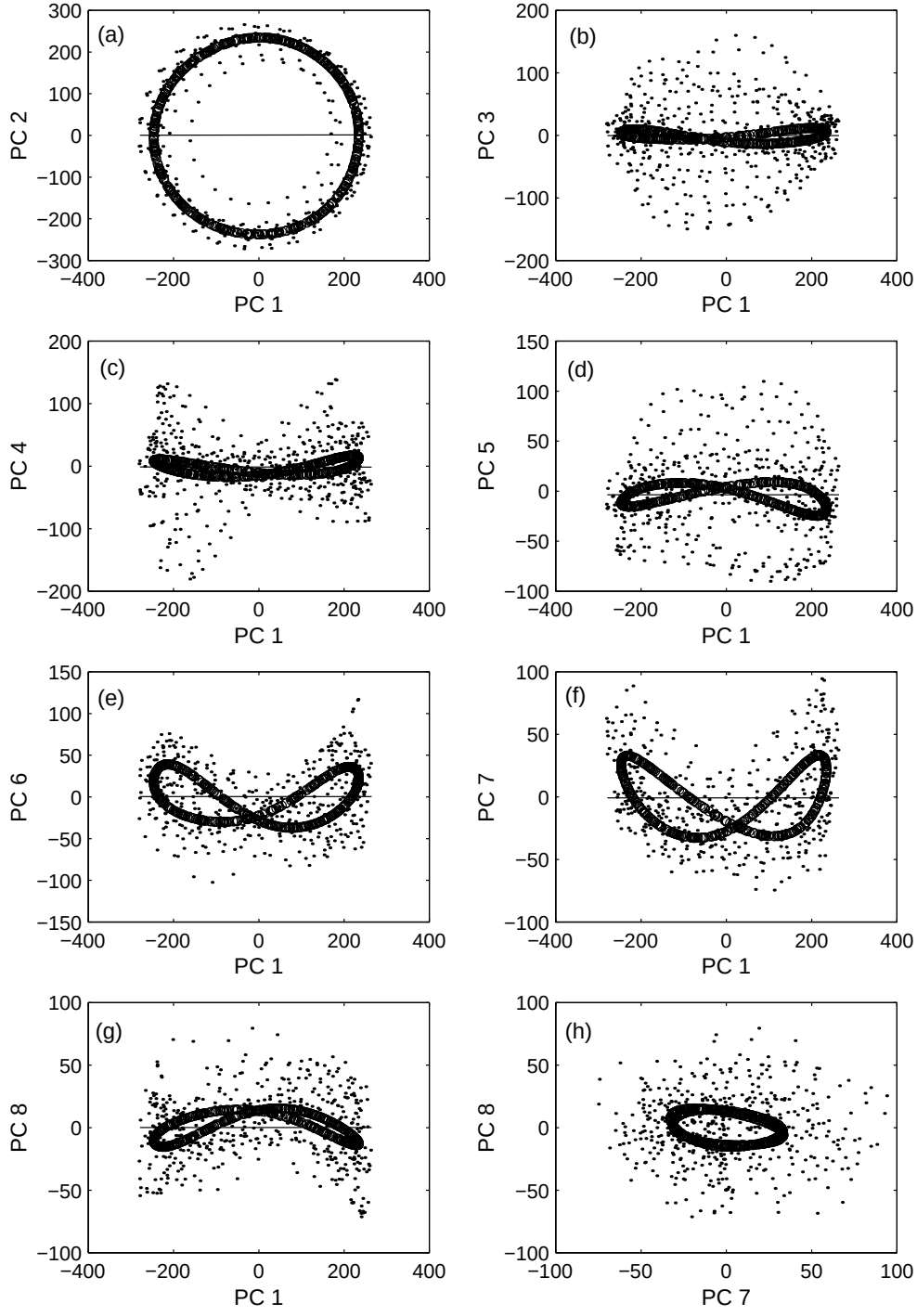

Figure 4. The NLSSA mode 1 solution is shown by the densely overlapping small circles (which tend to form a thick curve), while the data are shown as dots. For comparison, the PCA solution is shown as a thin straight line. Panels (a) to (g) show the solution in the PC1-PC2, . . ., PC1-PC8 plane, while panel (h) shows the PC7-PC8 plane. The solution is a twisted closed curve in the 8-dimensional PC space, but when projected onto a 2-dimensional plane, the curve often gives a false impression of self-intersection.

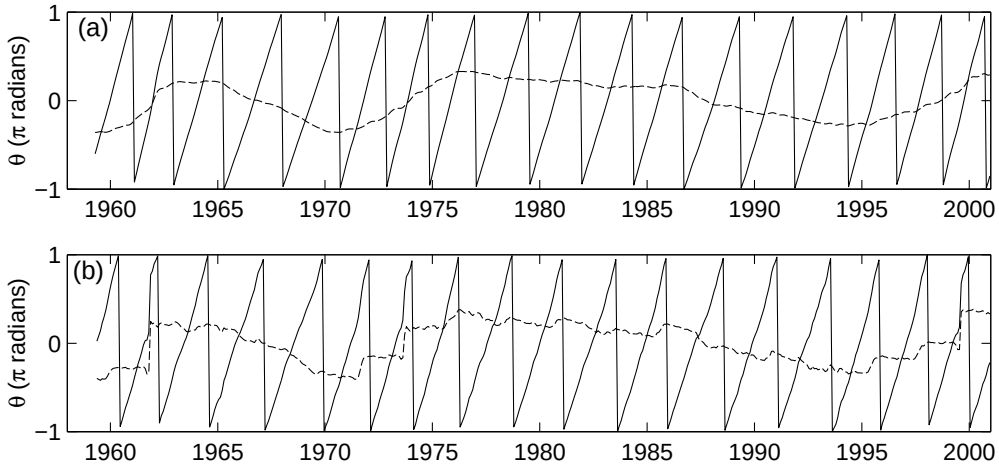

Figure 5. The mode 1 nonlinear principal component θ for (a) the zonal wind anomalies, and (b) the zonal acceleration, plotted as a function of time. Note θ (plotted in π radians) is a cyclic variable bounded between $(-1, 1]$. The steady linear increase over the entire record in θ with time was removed to give the θ anomalies, shown as dashed curves in (a) and (b).

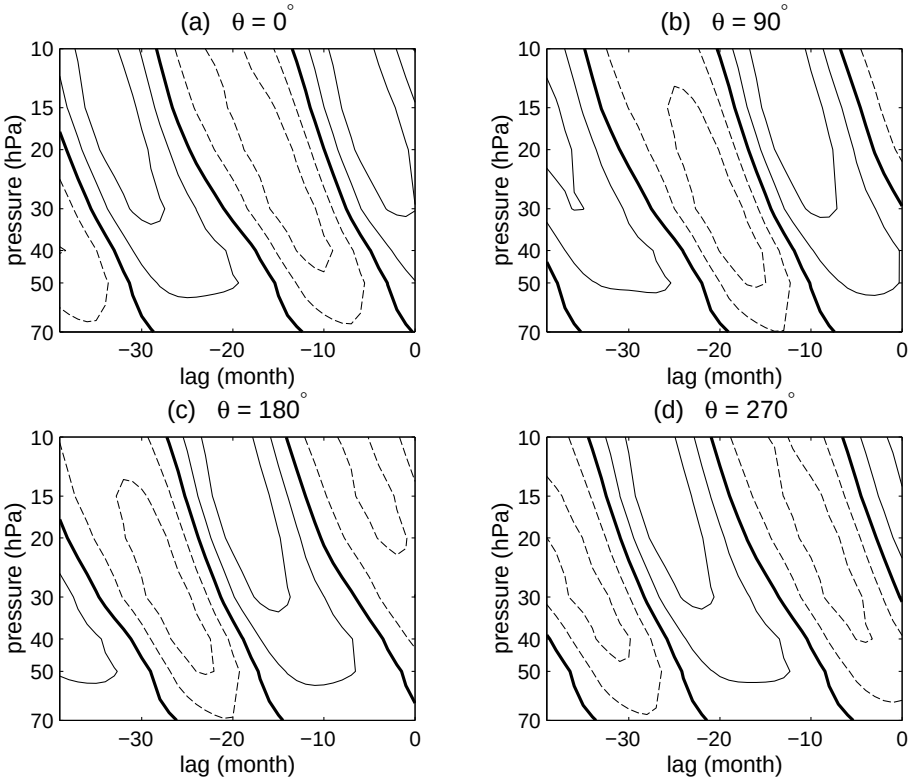

Figure 6. The NLSSA mode 1 loading patterns for the zonal wind anomalies as θ varies from (a) 0°, (b) 90°, (c) 180° to (d) 270°. Negative (easterly) contours are dashed, while the zero contour is thickened. Contour intervals are 10 ms^{-1}.

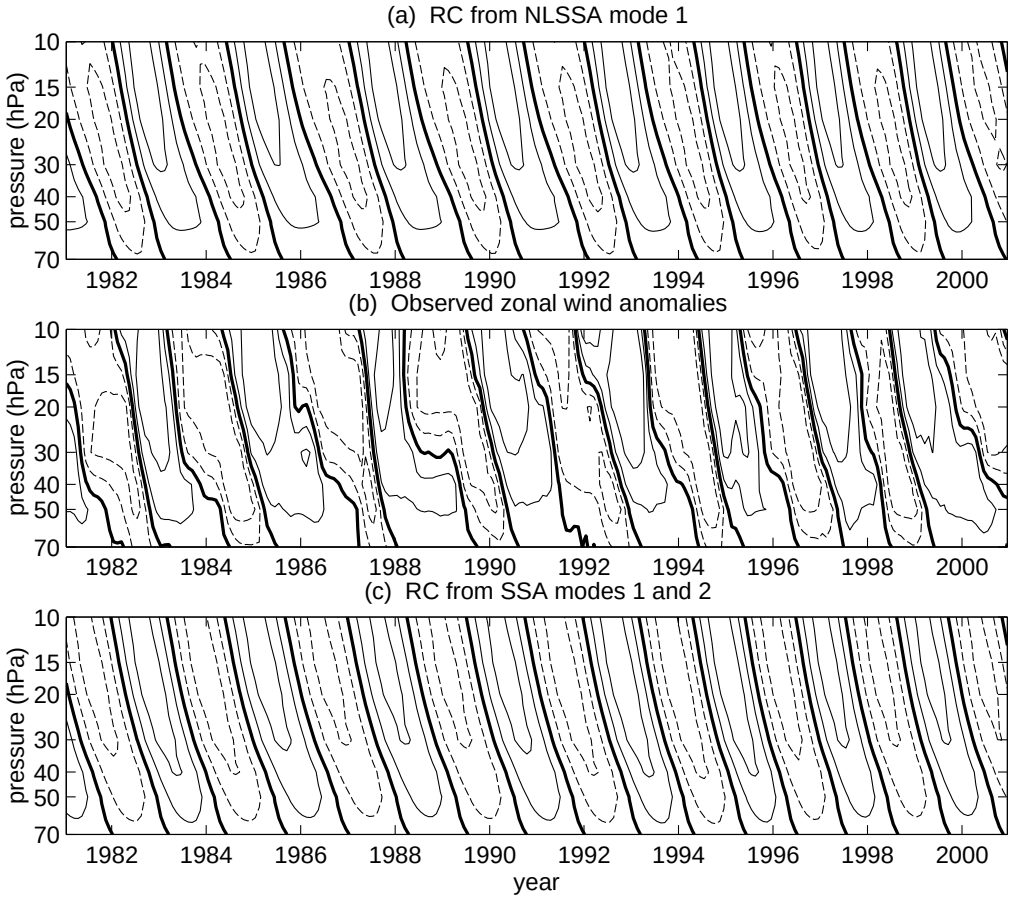

Figure 7. (a) The reconstructed component (RC) from NLSSA mode 1, (b) the observed zonal wind anomalies, and (c) the RC from the SSA modes 1 and 2. Only the period 1981-2000 is shown. The observed anomalies were smoothed by a 3-month running mean for better legibility. Negative (easterly) contours are dashed, while the zero contour is thickened. Contour intervals are 10 ms^{-1}.

4. NLSSA of the acceleration of the zonal wind

The observed QBO can also be characterized from the time series of the rate of change of the prevailing zonal wind, typically estimated by differencing monthly-mean data between consecutive months. As part of the present project, SSA was applied to this zonal acceleration time series. The leading eight SSA eigenvectors for the zonal acceleration accounted for 16.4, 16.0, 2.9, 2.8, 2.5, 2.4, 2.1, and 2.1%, respectively, of the variance— cumulatively, 47.2% of the variance. The eigenvectors of these leading 8 modes are shown in Fig. 8. Again, the first pair of modes have a time scale of about 28 months, that of the QBO. Modes 3 and 4 display oscillations about the 14-15 month period, close to the first harmonic. Modes 5 and 6 manifest oscillations mainly around the 12-month period, while modes 7 and 8 oscillate around the 9-10 month period. These determinations of the time scale for the modes agree with determinations made using the SSA PC time series (not shown).

The NLSSA mode 1 solution (Fig. 9) shows the main relation in the PC-space is the cyclic relation between PC1 and PC2. In contrast to the analysis for the zonal wind (Fig.

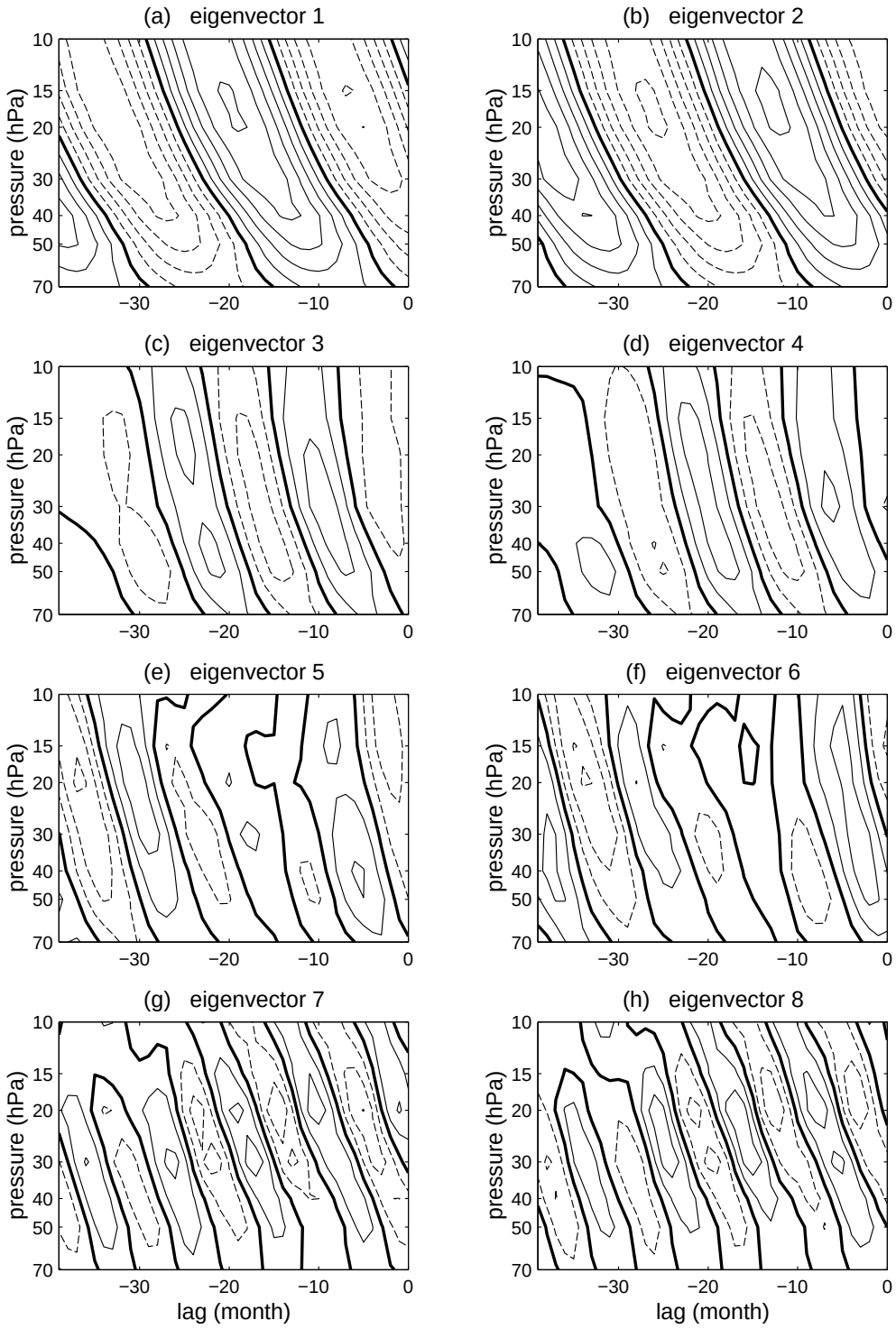

Figure 8. The leading eight SSA eigenvectors for the zonal acceleration. The eigenvectors are normalized to unit norm. Contour intervals are 0.02 in (a) and (b), and 0.05 in panels (c)-(h).

4), the PC3 and PC4 here display strong relations with PC1. As PC3 and PC4 oscillate at essentially the first harmonic of the 28-month period associated with PC1 and PC2, this reflects the strong relation between the basic QBO in the acceleration and its first harmonic. Furthermore, PC5, . . . , PC8 all manifest strong relations with PC1. Finally, a cyclic relation between PC7 and PC8 can also be seen (Fig. 9h). The time series for the nonlinear principal component θ is shown in Fig. 5b, with the departure from the steady increase in θ with time also shown as a dashed curve.

Comparing the NLSSA mode 1 loading patterns for various θ values (Fig. 10) with eigenvectors 1 and 2 (Fig. 8), we note that the nonlinear mode has more asymmetry between the westerly (eastward) and easterly (westward) acceleration, with the westerly acceleration of shorter duration but greater intensity. The tendency in the observed QBO for the downward descent of the easterly transitions to often stall for several months around the 30 hPa level is also captured nicely in the NLSSA mode 1. None of these subtleties can be seen in the SSA modes (Fig. 8).

The observed zonal acceleration, the RC from NLSSA mode 1 (NLRC1), and the RC from SSA modes 1 and 2 (RC1+2) are shown for the period 1981-2000 at the 40 hPa level in Fig. 11. The observed westerly (eastward) accelerations are usually more intense than the easterly ones. While neither NLRC1 nor RC1+2 can match the intense acceleration peaks in the raw observations, RC1+2 displays a near-sinusoidal variation that is very unlike the observations. NLRC1 does a much better job of capturing the strongly anharmonic nature of the acceleration time series, particularly the concentrated periods of westerly acceleration.

The correlation (averaged over all 7 levels) is 0.639 between the NLRC1 and the observations, and 0.559 between the RC1+2 and observations. The average RMSE is 4.18 $\mathrm{ms}^{-1}\mathrm{month}^{-1}$ for the NLRC1, and 4.49 $\mathrm{ms}^{-1}\mathrm{month}^{-1}$ for the RC1+2.

5. Conclusions

The NLSSA has been applied to a long time series of observations of the equatorial stratospheric zonal wind. In particular, the 8 leading SSA PCs of the zonal wind were computed and then input into an NLPCA.cir network. The NLPCA.cir produced a 1-D curve fit to the data in the 8-D PC space. This NLSSA solution when projected onto the 2-D plane spanned by two PCs revealed the relation between the two SSA PCs. The NLSSA mode 1 loading patterns showed that the easterly winds descended further down the atmosphere than the westerly winds. The NLSSA was then applied to study the zonal accelerations, where even stronger nonlinear relations were found among the leading 8 SSA PCs. The NLSSA mode 1 loading patterns displayed westerly (eastward) accelerations which were generally of shorter duration but greater intensity than the easterly (westward) accelerations (which often tended to stall in the downward descend).

From this and the earlier study by Hsieh and Wu (2002), we learned that the NLSSA has several advantages over the SSA: (a) While the PCs from different SSA modes are uncorrelated, they may have relations which are readily detected by the NLSSA. (b) Although the SSA modes are not restricted to sinusoidal oscillations in time like the Fourier spectral components, they are nevertheless inefficient in modelling strongly anharmonic oscillations like the QBO, scattering the signal energy into many SSA modes. The NLSSA recombines the SSA modes to extract the anharmonic signal. (c) As different SSA modes are associated with different time scales, the relations found by the NLSSA reveal the time scales among which there are interactions. For the QBO wind, there were interactions between the basic QBO time scale of about 28 months and the first harmonic at 14 months, and between 28 months and 12 months.

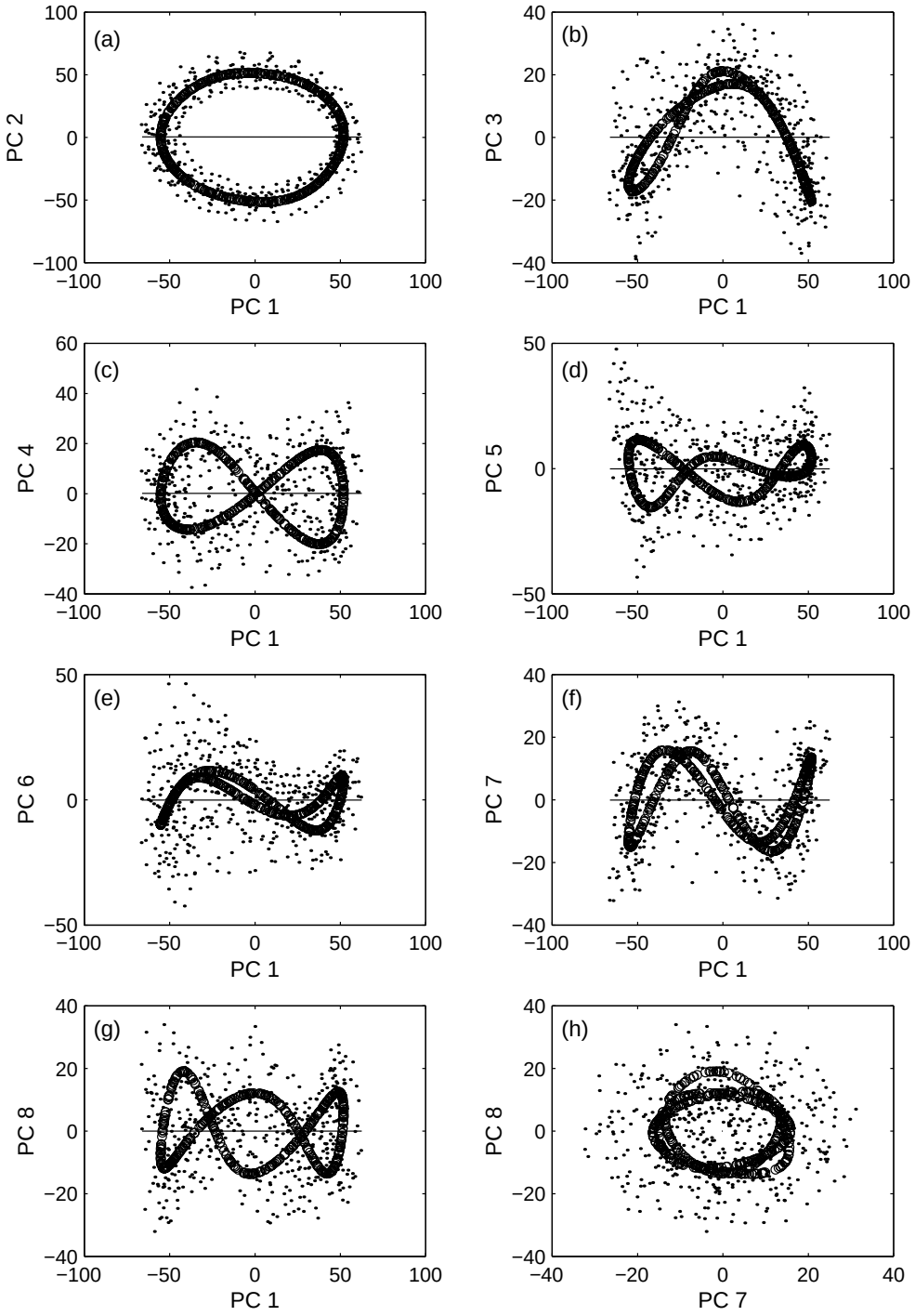

Figure 9. The NLSSA mode 1 solution for the zonal acceleration is shown by the (densely overlapping) circles, while the data are shown as dots. For comparison, the PCA solution is shown as a thin straight line. Panels (a) to (g) show the solution in the PC1-PC2, ..., PC1-PC8 plane, while panel (h) shows the PC7-PC8 plane.

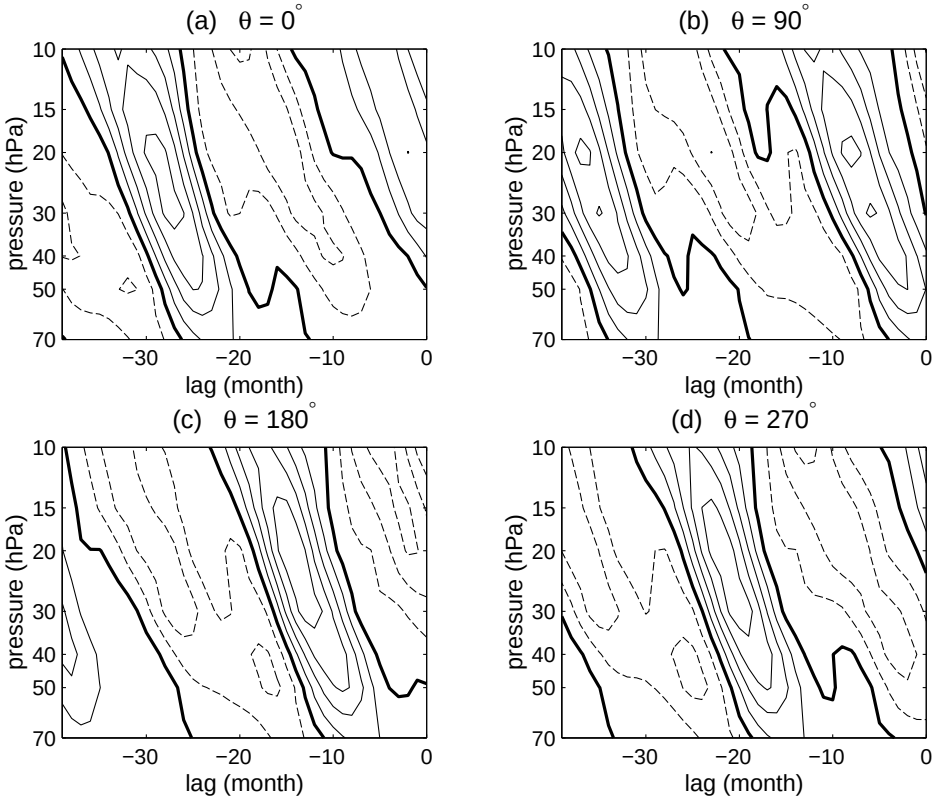

Figure 10. The NLSSA mode 1 loading patterns for the zonal acceleration as θ varies from (a) 0°, (b) 90°, (c) 180° to (d) 270°. Negative (i.e. easterly or westward acceleration) contours are dashed, while the zero contour is thickened. Contour intervals are 2 $\mathrm{ms}^{-1}\mathrm{month}^{-1}$.

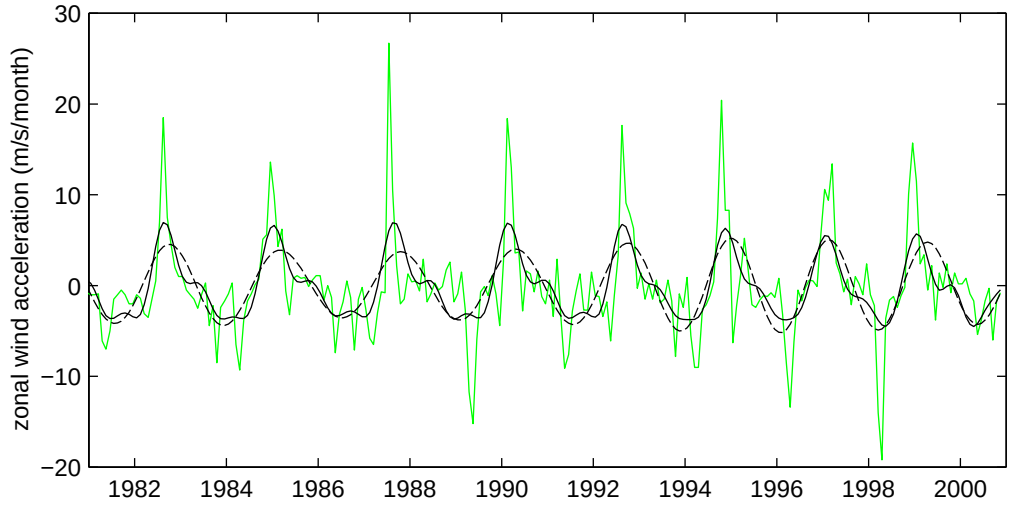

Figure 11. The observed 40 hPa zonal acceleration anomalies (light curve), the reconstructed component (RC) from NLSSA mode 1 (solid), and the RC from the SSA modes 1 and 2 (dashed). Only the period 1981-2000 is shown. The observed anomalies were smoothed by a 3-month running mean for better legibility.

Acknowledgement

The wind data were kindly provided by Barbara Naujokat of the Free University of Berlin. W. Hsieh was supported by research and strategic grants from the Natural Sciences and Engineering Research Council of Canada. The International Pacific Research Center at the University of Hawaii is supported in part by the Frontier Research System for Global Change.

Appendix

In the NLPCA.cir model (Fig. 1), the jth neuron $v_j^{(k)}$ in the kth layer ($k = 1, 2, 3, 4$, with the input layer being the 0th layer) receives its value from the neurons $\mathbf{v}^{(k-1)}$ in the preceding layer, i.e. $v_j^{(k)} = f_k(\mathbf{w}_j^{(k)} \cdot \mathbf{v}^{(k-1)} + b_j^{(k)})$, where $\mathbf{w}_j^{(k)}$ is a vector of weight parameters and $b_j^{(k)}$ a bias parameter, and the transfer functions f_1 and f_3 are the hyperbolic tangent functions, while f_2 and f_4 are simply the identity functions. Hence a total of 4 successive layers of transfer functions are needed to map from the inputs $\mathbf{x}$ to the outputs $\mathbf{x}'$. The bottleneck contains two neurons p and q confined to lie on a unit circle, i.e. only 1 degree of freedom as represented by the angle θ, which is the nonlinear principal component. To make the outputs as close to the inputs as possible, the cost function $J = \langle \|\mathbf{x} - \mathbf{x}'\|^2 \rangle$ (i.e. the MSE) is minimized (where $\langle \cdots \rangle$ denotes a sample or time mean). Through the minimization, the values of the weight and bias parameters are determined.

Because of local minima in the cost function, an ensemble of 30 NNs with random initial weights and bias parameters was run. Also, 20% of the data was randomly selected as test data and withheld from the training of the NNs. Runs where the MSE was larger for the test dataset than for the training dataset were rejected to avoid overfitted solutions. Then the NN with the smallest MSE was selected as the solution.

Hsieh (2001) noted that the NLPCA.cir, with its ability to extract closed curve solutions, is particularly ideal for extracting periodic or wave modes in the data. In SSA, it is common to encounter periodic modes, each of which had to be split into a pair of modes (Elsner and Tsonis 1996), as the underlying PCA technique is not capable of modelling a periodic mode (a closed curve) by a single mode (a straight line). Thus, two SSA modes can easily be combined into one NLPCA.cir mode. Hsieh (2001) pointed out that the general configuration of the NLPCA.cir is actually not restricted to modelling closed curve solutions, but may also represent open curve solutions like the original Kramer (1991) NLPCA. The reason is that the θ values computed by the NLPCA.cir network need not cover the full 360 degrees, hence the input $\mathbf{x}$ may be mapped into an open curve $\mathbf{x}'$.

To greatly reduce the number of input variables to the network, the original data were first analyzed by the SSA. Only the first few leading SSA modes are retained, and their PCs are then served as input variables to the NLPCA.cir network. The NLPCA.cir finds a continuous curve solution by nonlinearly relating the PCs, thereby giving the NLSSA mode 1.

The first 8 PCs from the SSA of the zonal wind data are inputted into the NLPCA.cir network (Fig. 1), with m, the number of hidden neurons in the encoding layer (and in the decoding layer) varying from 2 to 8. Validating the MSE over independent data not used in the training and testing process, we found the MSE to decrease readily as m increased from 2 to 4, but to fluctuate by no more than 0.5% as m increased from 4 to 8. Based on the principle of parsimony, the $m = 4$ solution was chosen as the most appropriate one,

and presented in Section 3. Due to the very strong signal to noise ratio in this dataset, no weight penalty (Hsieh 2001) was needed in the cost function.

For the zonal wind acceleration data, the same calculation was performed in Section 4, but with the $m = 6$ solution chosen.

References

Allen, M. R. and Smith, L. A. 1997 Optimal filtering in singular spectrum analysis *Phys. Lett. A*, **234,** 419-428

Baldwin, M., Gray, L., Dunkerton, T., Hamilton, K., Haynes, P., Randel, W., Holton, J., Alexander, M., Hirota, I., Horinouchi, T., Jones, D., Kinnersley, J., Marquardt, C., Sato, K. and Takahashi, M. 2001 The quasi-biennial oscillation. *Rev. Geophys.*, **39,** 179–229

Belmont, A. D. and Dartt, D. G. 1968 Variation with longitude of the quasi-biennial oscillation. *Mon. Wea. Rev.*, **96,** 767-777

Elsner, J. B. and Tsonis, A. A. 1999 *Singular Spectrum Analysis*, Plenum

Fraedrich, K., Pawson, S. and Wang, R. 1993 An EOF analysis of the vertical-time delay structure of the quasi-biennial oscillation. *J. Atmos. Sci.*, **50,** 3357–3365

Ghil, M., Allen, M. R., Dettinger, M. D., Ide, K., Kondrashov, D., Mann, M. E., Robertson, A. W., Saunders, A., Tian, Y., Varadi, F. and Yiou, P. 2002 Advanced spectral methods for climatic time series. *Rev. Geophys.*, **40,** DOI: 10.1029/2000RG000092

Hamilton, K. 1998 Dynamics of the tropical middle atmosphere: A tutorial review. *Atmos.-Ocean*, **36,** 319–354

Hamilton, K. and Hsieh, W. W. 2002 Representation of the QBO in the tropical stratospheric wind by nonlinear principal component analysis. *J. Geophys. Res.*, **107(D15),** DOI: 10.1029/2001JD001250

Hannachi, A. and Allen, M. R. 2001 Identifying signals from intermittent low-frequency behaving systems *Tellus*, **53A,** 469-480

Hsieh, W. W. 2001 Nonlinear principal component analysis by neural networks, *Tellus*, **53A,** 599-615

Hsieh, W. W. and Wu, A. 2002 Nonlinear multichannel singular spectrum analysis of the tropical Pacific climate variability using a neural network approach. *J. Geophys. Res.*, **107(C7),** DOI: 10.1029/2001JC000957

Jenkins, G. M. and Watts, D. G. 1968 *Spectral Analysis and its Applications*, Holden-Day

Kirby, M. J. and Miranda, R. 1996 Circular nodes in neural networks. *Neural Comp.*, **8,** 390–402

Kramer, M. A. 1991 Nonlinear principal component analysis using autoassociative neural networks. *AIChE Journal*, **37,** 233–243

Marquardt, C. and Naujokat, B. 1997 An update of the equatorial QBO and its variability. *World Meteorological Organization Technical Document No.814*, 87–90

Monahan, A. H. 2001 Nonlinear principal component analysis: Tropical Indo-Pacific sea surface temperature and sea level pressure. *J. Climate*, **14,** 219–233

Naujokat, B. 1986 An update of the observed quasi-biennial oscillation of the stratospheric winds over the tropics. *J. Atmos. Sci.*, **43,** 1873–1877

Wang, R., Fraedrich, K. and Pawson, S. 1995 Phase-space characteristics of the tropical stratospheric quasi-biennial oscillation. *J. Geophys. Res.*, **52,** 4482–4500

Wallace, J. M., Panetta, L. and Estberg, J. 1993 A phase-space representation of the equatorial stratospheric quasi-biennial oscillation. *J. Atmos. Sci.*, **50,** 1751–1762